



Noninvasive measurement of dielectric properties in layered structure: A system identification approach

R.M. Irastorza^a, M. Mayosky^b, F. Vericat^{a,c,*}

^a Instituto de Física de Líquidos y Sistemas Biológicos (IFLYSIB), CCT-La Plata-CONICET, UNLP, CICPBA, La Plata, Argentina

^b Laboratorio de Electrónica Industrial, Control e Instrumentación (LEICI), Facultad de Ingeniería, Universidad Nacional de La Plata (UNLP), La Plata, Argentina

^c Grupo de Aplicaciones Matemáticas y Estadísticas de la Facultad de Ingeniería (GAMEFI), UNLP, La Plata, Argentina

ARTICLE INFO

Article history:

Received 27 March 2008

Received in revised form 3 June 2008

Accepted 4 June 2008

Available online 12 June 2008

Keywords:

Open ended coaxial lines

Dielectric measurements in layered lossy structure

System identification

Time domain reflectometry

ABSTRACT

In this paper, estimation of the dielectric properties of layered lossy structure using open-ended coaxial probes is analyzed. Theoretical and empirical exponential approximations of the relaxation process are generalized for two, three and four-layers structures. As measurements are taken in the 10 MHz to 1 GHz frequency range, a wide frequency spectrum measurement procedure is proposed, providing a fast method to approximate parameters (thickness and dielectric properties) of each layer. Application of the methodology depends on some prior knowledge of the properties of the dielectric layers (i.e. number of layers and approximate values of their thicknesses and permittivities). A linear System Identification method is proposed using time domain measurements to find the corresponding frequency responses. Although these approaches and techniques have been already considered individually, they are combined here, resulting in a novel methodology to process time domain reflectometry data that is robust and numerically well-behaved. Simulations and experimental results in phantom and a biological tissue are provided. Dielectric relaxation is assumed to follow a Debye model, but comments on other parameterizations are also summarized. Experimental frequency validation data are reliable up to 700 MHz.

© 2008 Elsevier Ltd. All rights reserved.

1. Introduction

Changes in physiological properties (e.g.: composition [1], mineral content [2], tissue water content [3–6], thickness) of biological tissues can provide significant information from a clinical point of view. In some cases, these variations produce changes in the dielectric properties of the medium under measurement (MUM). For instance, the stratum cornea water content *in vivo* can be estimated by dielectric measurements [7]. In [8] it is shown that the dielectric constant of subcutaneous fat goes from 25 for normal skin to 10 for severe subcutaneous fibrosis. Besides, a correlation of this dielectric constant with local oedema,

swollen tissue problems and fluid retention in humans is also found. In bone tissues, variation in collagen content is strongly correlated to relative permittivity [1]. Furthermore, changes in relaxation frequencies for natural and demineralized bones are reported in [2,9].

Open ended coaxial lines (OECL) have been successfully used for measuring dielectric properties of layered materials [10–12]. Their wide frequency response allows the study of different dielectric relaxation processes, providing relevant information not achievable with other kind of probes. As a non-invasive technique, it is well suited for application in biological measurements *in vivo*, without damaging the material under test [3,5]. The measurement configuration used in this work, shown in Fig. 1, can be applied not only for biological tissues but also in many industrial processes [10,13].

In search of suitable models, several authors have developed mathematical [14,15], empirical [3,4,16,17]

* Corresponding author. Address: Instituto de Física de Líquidos y Sistemas Biológicos (IFLYSIB), CCT-La Plata-CONICET, UNLP, CICPBA, La Plata, Argentina.

E-mail address: vericat@iflysib.unlp.edu.ar (F. Vericat).

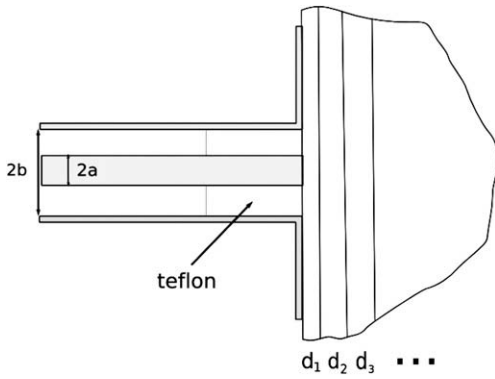


Fig. 1. Probe in contact with a layered geometry.

and numerical [18] approaches. In particular, in this paper the method presented by Alanen et. al [3] is used and extended to a four layer structure. The simple exponential approximation is also tested and generalized. The resulting approach is useful to represent measurements of stratified biological tissues that can be dielectrically modeled by layers and to rapidly observe the behavior of the apparent permittivity relaxation frequencies.

Time domain reflectometry (TDR), combined with OECL, has been extensively used to obtain dielectric properties of materials [19,7]. One of its advantages is the wide band spectrum that can be ideally achieved in a single measurement using Fourier transform techniques. Nevertheless, in practice this is a rather complicated problem (see Section 2.3 and [20,21]). In this paper, we propose System Identification tools [22–24] that avoid this problem and result in a fast and robust analysis of TDR data. The technique imposes that the structure under measurement is modeled as a causal linear time invariant (CLTI) system. Application of the proposed methodology depends on a previous knowledge of the kind of tissues under study and hence, on the expected values their dielectric properties can take. Deviations from these values can suggest abnormal conditions. A physical lumped differential circuit model is used [25], which results in a numerically well-behaved approach.

The aim of this work is to adapt and test the System Identification approach as a general signal processing technique to analyze TDR data. A generalization of the non-invasive multi-layered OECL model is proposed, and a methodology to obtain fast and robust measurements in stratified lossy material is developed.

Paper is organized as follows. In Sections 2.1 and 2.2 a short overview of the theoretical and the empirical model of the apparent permittivity using open ended coaxial lines is presented, and the corresponding equations for a four layered structure are developed. In Section 2.3 the lumped circuit model used is reviewed and a brief introduction of Orthonormal Bases identification methods [24] is given. The exponential approximations, together with the physical model already mentioned, are used to match the physical boundary conditions of the identification methodology. Finally, in Sections 3 and 4, simulations with literature values, phantom, and biological layered tissue measurements are reported.

2. Theory

2.1. Theoretical model

The static capacitance of an arbitrary structure with two conductors at potential zero and V_0 , respectively [3], can be expressed as follows:

$$C = \frac{1}{V_0^2} \int_V \varepsilon (\Delta V)^2 dv, \quad (1)$$

where v is the volume of the capacitor, V is the electric potential and ε is the permittivity of the material under measurement. It is assumed that the system operates at such a frequency that only the fundamental TEM mode propagates in the coaxial line. Evanescent TM_{0n} modes are also assumed to exist in the coaxial line near the probe end. This is necessary to match boundary conditions at the probe-material contact and between each layer interface. According to the assumptions and formulations in [3], the capacitance of an OECL in contact with either a half-infinite material or a layered geometry is given by

$$C = \frac{2\pi\varepsilon_1\varepsilon_0}{V_0^2} (P_{00} + 2g_1P_{01} + 2g_2P_{02} + 2g_1g_2P_{21} + \dots + g_1^2P_{11} + g_2^2P_{22} + \dots) + 2\pi\varepsilon_t\varepsilon_0 \sum_{i=1}^l g_i^2 p_i t_i \quad (2)$$

for $l = 2$, coefficients g_i are solved from:

$$\begin{bmatrix} P_{11} - V_0^2 \frac{\varepsilon_t}{\varepsilon_1} p_1 t_1 & P_{12} \\ P_{21} & P_{22} - V_0^2 \frac{\varepsilon_t}{\varepsilon_1} p_2 t_2 \end{bmatrix} \begin{bmatrix} g_1 \\ g_2 \end{bmatrix} = \begin{bmatrix} -P_{01} \\ -P_{02} \end{bmatrix}, \quad (3)$$

where:

$$t_i = \frac{b^2}{2} [\alpha_i J_1(p_i b) + \beta_i Y_1(p_i b)]^2 - \frac{a^2}{2} [\alpha_i J_1(p_i a) + \beta_i Y_1(p_i a)]^2.$$

J_i and Y_i are the Bessel functions of the first and second kind. The coefficients α_i , β_i and p_i are determined numerically from the boundary conditions: $T_i(a) = T_i(b) = 0$, where $T_i(\rho) = \alpha_i J_0(p_i \rho) + \beta_i Y_0(p_i \rho)$ and the normalization condition $\alpha_i^2 + \beta_i^2 = 1$. The coefficients P_{mn} depend on the material under test and the number of layers. This result can be extended for a four layered structure and the respective definitions of Eqs. (2) and (3) are shown in Appendix A.

In the above formulations it should be noted that the electrostatic model approximation limits the frequency range. Therefore probe dimensions should be much smaller than the wavelength in the tissues, in other words $2a/\lambda \ll 1$.

2.2. The empirical model

As noted in the previous section, the permittivities of each layer can not be directly solved, see Eq. (2). Hence, iterative methods must to be used. In [3] an *empirical approximation* was proposed. Under some assumptions, it allows solving the apparent complex dielectric permittivity (ε_{app}^*) seen by the probe:

$$\varepsilon_{app}^* = \frac{C - C_f}{C_0}, \quad (4)$$

where the coefficients C_0 and C_f are determined from calibration measurements. Although the theoretical capacitance is a more exact expression Eq. (2), it implies numerical integration, which is not convenient in practice. The value of the sample permittivity can be easily solved from Eq. (4). This empirical model can also be used to estimate the apparent complex permittivity (ϵ_{app}^*) of an open ended coaxial line in contact with a layered geometry (see [3]). The equations for a bi-layered structure are

$$\epsilon_{\text{app}}^* = (\epsilon_1 - \epsilon_2)(1 - e^{-qd}) + \epsilon_2 \quad \text{when } \epsilon_1 > \epsilon_2, \quad (5)$$

$$\frac{1}{\epsilon_{\text{app}}^*} = \left(\frac{1}{\epsilon_1} - \frac{1}{\epsilon_2} \right) (1 - e^{-qd}) + \frac{1}{\epsilon_2} \quad \text{when } \epsilon_1 < \epsilon_2, \quad (6)$$

where q is a constant depending on the probe size. As the formula to be applied depends on the material under test, an *a priori* estimation of each layer permittivity value is required. In [3] the empirical formulas are extended for a particular three-layer model, taking into account skin dielectric values. In this work the empirical formula is extended to other three-layered structure and also to a four-layer model, by combining the above equations. The permittivity value estimations chosen for each layer are similar to those to be used in the experimental set-up of Section 4, resulting:

$$\epsilon_{2-4}^* = \epsilon_2(1 - e^{-q_2d_2}) + \frac{\epsilon_3\epsilon_4}{\epsilon_3e^{-q_3d_3} + \epsilon_4(1 - e^{-q_3d_3})} e^{-q_2d_2}, \quad (7)$$

$$\epsilon_{\text{app}}^* = \frac{1}{(1 - e^{-q_1d_1}) \left(\frac{1}{\epsilon_1} - \frac{1}{\epsilon_{2-4}^*} \right) + \frac{1}{\epsilon_{2-4}^*}}, \quad (8)$$

q_1 , q_2 and q_3 are constants generally found by numerical fitting with Eq. (2).

It should be remarked that assuming a Debye (lossy material) behavior of the sample:

$$\epsilon_i^*(j\omega) = \epsilon_\infty + \frac{\Delta\epsilon}{1 + j\frac{\omega}{\omega_r}}, \quad (9)$$

where $\Delta\epsilon = \epsilon_s - \epsilon_\infty$, Eqs. (4)–(8) can be seen as rational stable functions of frequency.

2.3. System identification approach

The measurement procedure proposed involves identification of a linear relation between a step voltage applied to the MUM (input) and the corresponding reflected wave (output). Considering $f_2(t)$ as the difference between sample and short circuit and $f_3(t)$ as the difference between open circuit and sample, a CLTI system approximation can be stated [2]:

$$H(s) = C_0 Z_0 \epsilon(s) + \frac{f_3(\infty)}{f_2(\infty)s} = \frac{F_3(s)}{sF_2(s)}, \quad (10)$$

where $F_2(s)$ and $F_3(s)$ are the Laplace transform of $f_2(t)$ and $f_3(t)$, respectively, and s is the Laplace variable. C_0 and Z_0 are the cell capacity and characteristic impedance, respectively. Although the method were developed and tested for invasive measurements [2], it is possible to apply the same reasoning to non-invasive OECL. Assuming a Debye (or constant) behavior of each layer, replacing $\epsilon(s)$ by $\epsilon_{\text{app}}(s)$ and taking an empirical formula (for instance Eq. (8)) a CLTI system is obtained. It should be noted that the poles of this system are coincident with those of $\epsilon_{\text{app}}(s)$.

From the above results, the problem reduces to estimating the transfer function of the CLTI system Eq. (10). This may be done by a simply division of numerical Fourier transforms of $f_2(t)$ and $f_3(t)$. However, in practice, the measured data are corrupted by errors due to measurements errors, noise, etc. This often yields divergent results ([20,21]). Here a System Identification technique is used, using $f_2(t)$ as input and the integral of $f_3(t)$ as the output. On the other hand, the transfer function of a CLTI system can be approximated by the following equation:

$$H(s) \approx \frac{n(s)}{d(s)} = \frac{n_0s^m + n_1s^{m-1} + \dots + n_m}{s^n + d_1s^{n-1} + \dots + d_n}, \quad (11)$$

where for stable transfer functions $m \leq n$. However, the nature of the problem imposes some additional restrictions to the degrees of $n(s)$ and $d(s)$. Actually, the boundary conditions are: $0 < \epsilon_{\text{app}_s} < \infty$ and $0 < \epsilon_{\text{app}_\infty} < \infty$ (where ϵ_{app_s} and $\epsilon_{\text{app}_\infty}$ are the limits for s tends to 0 and to ∞ , respectively) then $n = m$, $n_0 = -1$ and $d_n = n_m$. Further details are explained in [2].

Most identification methods are developed for discrete time systems. However, once the discrete system is identified, a continuous one can be obtained by any suitable conversion method (e.g. zero-order hold). Here we apply an Orthonormal Based with Fixed Poles (OBFP) model structure. It allows incorporation of *a priori* information of system dynamics in the identification process. Another advantage is that the input–output equation can be written as a linear regression and therefore the estimate is robust and consistent even when the model noise is not white. A detailed analysis of OBFP identification can be found in [24]. Generally speaking, output-error (OE) models can be expressed as

$$y_k = H_d(q)u_k + v_k, \quad (12)$$

where $H_d(\bullet)$ is the discrete version of $H(s)$, q is the shift operator and y_k , u_k and v_k are the output, input and measurement noise vectors at time k (e.g. $y_k = y(kT_s)$, where T_s is the sample time), respectively. In the particular case of OBFP, Eq. (12) is defined as

$$y_k = \sum_{i=0}^{\infty} \mathbf{b}_i \mathcal{B}_i(q) u_k + v_k, \quad (13)$$

where \mathbf{b}_i are the unknown parameters and $\{\mathcal{B}_i(q)\}_{i=0}^{\infty}$ are rational orthonormal bases defined by

$$\mathcal{B}_\ell(q^{-1}) = \left(\frac{\sqrt{1-|\xi_\ell|^2}}{q^{-1}-\xi_\ell} \right) \prod_{i=0}^{\ell-1} \frac{1-\bar{\xi}_i q^{-1}}{q^{-1}-\xi_i}, \quad \ell > 0, \quad (14)$$

$$\mathcal{B}_0(q^{-1}) = \frac{\sqrt{1-|\xi_0|^2}}{q^{-1}-\xi_0},$$

where ξ_ℓ are stable modes ($|\xi_\ell| < 1$) arbitrary chosen.

In the OBFP identification process, modified routines developed in [24] are used. Matlab System Identification toolbox [23] routines were also used but results will not be shown here. In this particular case, the model structure chosen was OE model and no *a priori* information of the system dynamic can be assumed. As a result, excepting for the model order, an “almost” black-box model approach is applied. This identification method could be applied when there is a poor knowledge of system dynamics.

2.4. System validation

After a particular model is obtained its consistency must be verified, a process known in System Identification as model validation. In this work two validation tests are proposed: time and frequency validation. In the former the same input ($f_2(t)$) is applied to both the sample and the model, and their outputs are compared. In the latter the magnitude of the reflexion coefficient of the OECL with the MUM ($|\Gamma^*(s)|_{meas}$ with $s = j\omega$) is measured in the frequency range of interest and compared with the predicted values. Such comparison is performed by

$$FIT_f = 100 \frac{[1 - \text{norm}(|\Gamma^*(j\omega)|_{id} - |\Gamma^*(j\omega)|_{meas})]}{\text{norm}[|\Gamma^*(j\omega)|_{meas} - |\Gamma^*(j\omega)|_{meas}]}, \quad (15)$$

where $|\Gamma^*(j\omega)|_{id}$ is the magnitude of the reflection coefficient calculated with the resulting admittance of the identification process:

$$Y(j\omega)|_{id} = j\omega(C_0 \epsilon_{app}^*(j\omega)|_{id} + C_f). \quad (16)$$

A similar FIT definition is applied to the time validation test.

The whole identification procedure is summarized as follows:

- (1) Estimate dominant dynamics. For instance, in a three layer material, if $\epsilon_1 > \epsilon_2$ and $\epsilon_2 < \epsilon_3$, therefore Eq. (5) is applied for the first and second layer and then combined with Eq. (6) for the third. The (approximately known) parameters of each layer (thickness and dielectric properties) must be used.
- (2) Find the approximated discrete poles (of Eq. (10), through $\xi_\ell = \exp(p_\ell T_s)$, where the ξ_ℓ are the discrete poles, p_ℓ are the continuous ones and T_s is the sample period.
- (3) Generate the bases with the poles found in the previous step using Eq. (14).

- (4) Obtain a least square estimate and check the time and frequency Eq. (15) validation parameters. Repeat the previous steps if necessary.

It is worth noting that the identification method does not just imply fitting of the experimental data; it generates a linear model which approximates the dynamics of the real system under test.

3. Simulations

The process to find the empirical parameters of a layered geometry is similar to that applied in [3]. C_0 and C_f are previously calculated using the approximation $C(\epsilon_i) = -C_0 \epsilon_i + C_f$, where $C(\epsilon_i)$ is obtained by Eq. (2) applied to a semi-infinite material. In our case, two probes of different sizes were used ($2b = 10$ mm and $2b = 16$ mm). The resulting values for C_0 and C_f were: $6.4/8.5 \times 10^{-2}$ pF and $3.4/3.6 \times 10^{-2}$ pF, respectively. Then a fitting of the theoretical and empirical approaches (e.g. in a four layer structure Eqs. 2 and 8) is performed. The simulation values used are imposed by the biological material of interest and the experimental set-up and. For instance, Fig. 2 shows a comparison between the theoretical and the empirical approximation in a four layer structure with a 16 mm probe (it results in the Eq. 8). The thickness of the second layer (d_2) is changed from 0.6 mm to 1.8 mm and $d_1 = 0, 20, 40$ μm . The dielectric constant of the four layers were assumed to be 10, 50, 8 and 40. These values are consistent with calibration media values (see Section 4). Similar results were found when the other parameters were changed. The obtained values were: $0.86/0.75/0.56$ mm^{-1} and $0.54/0.74/0.61$ mm^{-1} for q_1, q_2 and q_3 for the 10 mm and 16 mm probes, respectively.

In Fig. 3 the three layer empirical model is tested for the 16 mm probe. First, the dielectric constant of the three layers were set in order to accomplish $\epsilon_1 > \epsilon_2$ and $\epsilon_2 < \epsilon_3$ (see

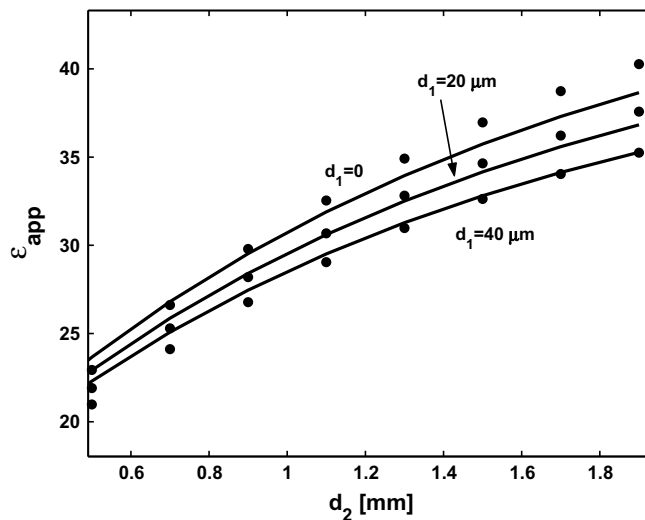


Fig. 2. Apparent dielectric constant of a four-layer structure seen by 16 mm probe. Variational method (full curves) and empirical approximation (dotted curves). The empirical parameters obtained were: $q_1 = 0.86$, $q_2 = 0.75$ and $q_3 = 0.56$.

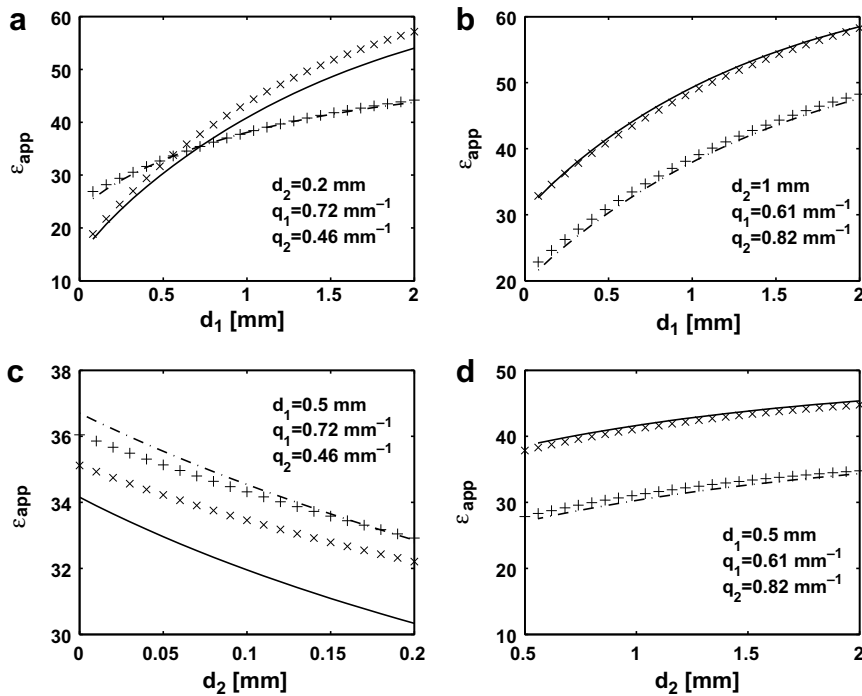


Fig. 3. Comparison between empirical (+ and × curves) and theoretical (full and dashed curves) model in a three layered geometry. In (a) and (c) $\epsilon_1 > \epsilon_2$ and $\epsilon_2 < \epsilon_3$ (the dielectric constant were assumed to be 70, 5, 20 (full curves) and 50, 10, 30 (dashed curves)). In (b) and (d) $\epsilon_1 > \epsilon_2$ and $\epsilon_2 > \epsilon_3$ (the dielectric constant were assumed to be 70, 40, 20 (full curves) and 70, 30, 10 (dashed curves)).

Fig. 3a and c). It is noted that the approximation is not so accurate when the lowest dielectric constant layer thickness is changed. Second, in Fig. 3b and d $\epsilon_1 > \epsilon_2$ and $\epsilon_2 > \epsilon_3$. A good agreement is observed in this case. It should be noted that the empirical parameters were different in the two configurations.

In the simulations performed, dielectric permittivities of each layer were set to constant values. In Fig. 4a and b a calibration geometry comprising saline solution (literature values of 0.45% NaCl and $d_1 = 0.5$ mm)/ nylon film ($\epsilon_2 = 3$ and $d_2 = 0.1$ mm)/ 2-propanol (see [26]) was simulated at $T = 25^\circ\text{C}$. Debye dielectrics (see Eq. 8) and a 10 mm probe were assumed. Linear system transfer functions Eq. (11) were directly fitted (in frequency domain) with the theoretical curve Eq. (2). It can be seen that with a system of order 2, the approximation is very bad. However, good results were obtained with systems of order 3 and 4. The empirical approximation is also shown and considering the formulations in Section 2.4, a 3 order system is obtained with an acceptable agreement. Fig. 4c and d show real and imaginary parts of the apparent permittivity of 1-propanol ($d_1 = 0.5$ mm)/nylon film $d_2 = 0.1$ mm/2-propanol. Note that the first and last layers have comparable complex permittivity values with relaxation frequencies of 474 and 434 MHz (literature values). Linear (directly fitted in frequency domain) and empirical models are in very close agreement with the theoretical one.

It is well known that dielectric properties of materials can be parameterized in frequency domain (Debye, Cole–Cole (C–D), Cole–Davidson (C–D) or more general Havriliak–Negami (H–N)) and in time domain (Kohlrausch–Wil-

liams–Watts (KWW), see [27]). As it was mentioned, if a Debye parameterization is assumed the material can be directly approximated by a CLTI system. Instead, with C–C, C–D, H–N and K–W–W dielectrics, non-linear systems are obtained. Fig. 5 shows their respective Cole–Cole plots and linear system approximations (directly fitted in frequency domain). In the identification procedure, assuming a semi-infinite material, step (1) must be modified (Section 2.4). For the general frequency model of a H–N dielectric, the complex permittivity could be approximated by

$$\begin{aligned} \epsilon_i^*(j\omega) &= \epsilon_\infty + \frac{\Delta\epsilon}{\left[1 + \left(j\frac{\omega}{\omega_{H-N}}\right)^{\alpha-1}\right]^\beta} \approx \frac{n(j\omega)}{d(j\omega)} \\ &= \frac{n_0(j\omega)^m + \dots + n_m}{(j\omega)^n + \dots + d_n} \end{aligned} \quad (17)$$

with $0 < \alpha < 1$ and $0 < \beta < 1$. Starting from some *a priori* known $\hat{\alpha}$ and $\hat{\beta}$, estimate the parameters n_i and d_i , by fitting theoretical curves to rational functions of $j\omega$. On the other hand, for a K–W–W time domain parameterization it was shown in [27] that there is an exact analytical Fourier transform defined as

$$\begin{aligned} \frac{\epsilon_i^*(j\omega) - \epsilon_\infty}{\Delta\epsilon} &= \begin{cases} 1 - \sum_{k=0}^{\infty} \frac{(-1)^k \Gamma(\frac{k+1}{\beta})}{\beta \Gamma(k+1)} (-j\omega\tau_\beta)^{k+1} & \text{when } |j\omega\tau_\beta| \rightarrow 0, \\ 1 - \sum_{k=0}^{\infty} \frac{(-1)^k \Gamma(\beta k+1)}{\Gamma(k+1)} (-j\omega\tau_\beta)^{-\beta k} & \text{when } |j\omega\tau_\beta| > 0, \end{cases} \end{aligned} \quad (18)$$

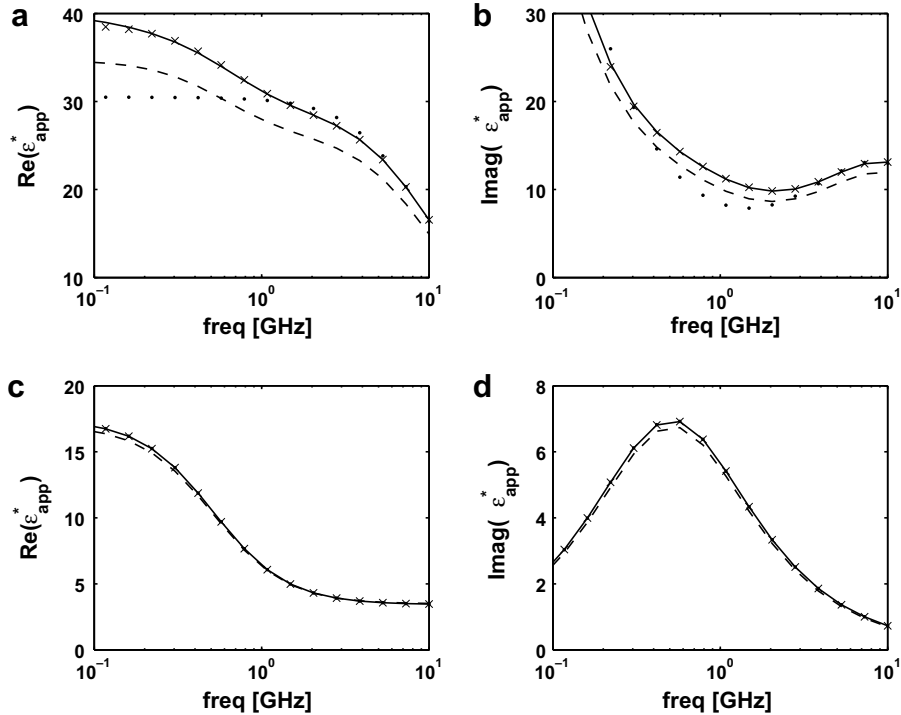


Fig. 4. Simulations of three layered structure with Debye dielectrics and their fitted linear systems. (a) and (b) real and imaginary part of $\epsilon_{app}^*(j\omega)$ of: saline solution/nylon film/2-propanol and its fitted systems ($m = n = 2$ and 3 in dotted and \times curves, respectively), theoretical (full curves) and empirical (dashed curves) models. (c) and (d) real and imaginary part of 1-propanol ($d_1 = 0.5$ mm)/nylon film $d_2 = 0.1$ mm/2-propanol. Fitted systems ($m = n = 2$ and 3 in dotted and \times curves, respectively), theoretical (full curves) and empirical (dashed curves) models.

where $\Gamma(x)$ denotes the complementary complete gamma function and $\frac{1}{\tau_p} = \omega_{r_{KWW}}$ is the relaxation frequency. Therefore Eq. (18) must be generated in order to fit it with a rational function, as in the frequency case. Fig. 5d shows simulations of Eq. (18) where series were truncated at $k = 200$. Linear systems were fitted, for this particular case a good agreement is observed for systems of order 8.

Limitations with non linear dielectric parametrizations can be summarized as follows:

- (1) Linear system estimation must be performed to estimate the dominant system dynamic.
- (2) If a K–W–W time domain parametrization is assumed, Eq. (18) must be calculated first.
- (3) The number of parameters that must be estimated is incremented.
- (4) System order is incremented.
- (5) If a semi-infinite sample is assumed, rational function poles (CLTI system, Eq. 17), in general, do not coincide with the relaxation frequencies of the dielectric, as in the linear system case.

It is remarked that in the theoretical simulations of the capacitances $C(\epsilon_i, d_i)$ (see Eq. 2), the series were truncated at $l = 3$ and the coefficients P_{ij} were numerically calculated with a Gauss–Newton algorithm.

4. Measurements and results

4.1. Phantom measurements

Multi-layer models were tested from 10 MHz to 1 GHz, by comparing simulated (with lossy materials of known electric properties, e.g.: water, saline solution and *n*-alcohols at 25 °C) and measured values. The experimental set-up is shown in Fig. 6. For instance, in a four layer geometry, the probe, covered with a nylon film, is attached to a liquid chamber filled with water and provided with a movable glass with a nylon film as bottom and filled with the alcohol to form a four-layer structure, nylon/water/nylon/alcohol. Since the alcohol layer is thick (10 mm) the fourth layer can be considered to have an infinite thickness.

A Hewlett–Packard TDR/Sampler 1815B plug in a Hewlett–Packard 1801A oscilloscope and a sampler head HP1106A with a tunnel diode HP1106 was used in the identification procedure. Therefore a fast step voltage (time rise of 35 ps.) was applied to the sample. The reflection coefficient magnitude of the probe attached to the media were also measured by a Scalar Network Analyzer (SNA) HP8711A from 10 to 1300 MHz. These data were used in the validation process. Two OECL with type N connector were manufactured to test our technique, with $2b = 10$ mm and 16 mm, respectively. Temperature was controlled by a cryostat LAUDA RE106.

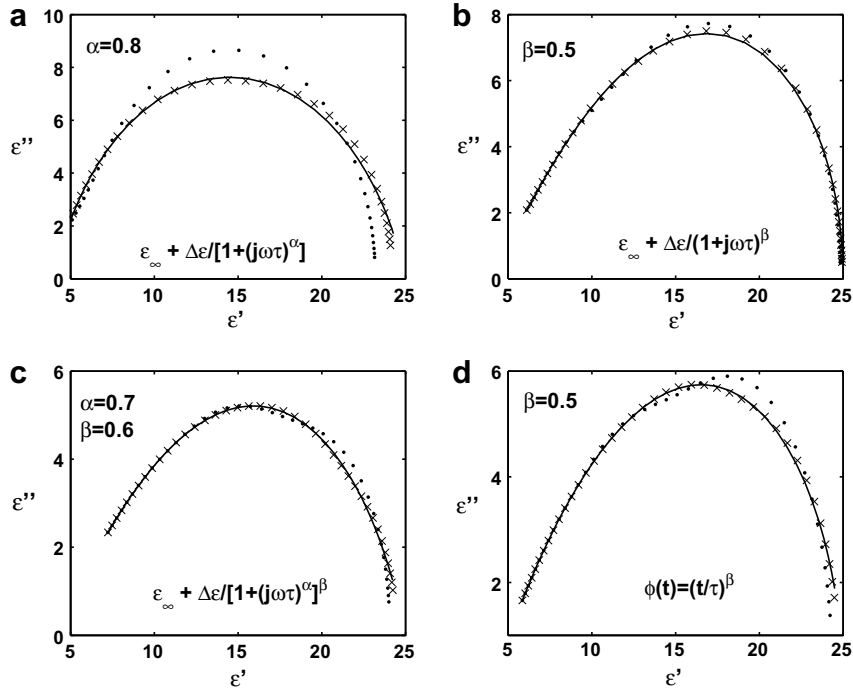


Fig. 5. Cole–Cole plots of non Debye dielectrics. In all figures parameters are defined as: $\epsilon_\infty = 4$, $\Delta\epsilon = 21$ and $\omega_r = \frac{1}{\tau} = 2\pi \times 10^8$. (a) Cole–Cole dielectric (full curve) and fitted linear systems of order: $m = n = 2$ and 5 (dotted and \times curves). (b) Cole–Davidson (full curve) and fitted linear systems of order: $m = n = 3$ and 4 , (dotted and \times curves). (c) Havriliak–Negami dielectric (full curve) and fitted linear systems of order: $m = n = 5$ and 8 . (d) Kohlrausch–Williams–Watts dielectric (with series truncated at $k = 200$) (full curve) and fitted linear systems of order $m = n = 5$ and 8 for (dotted and \times curves).

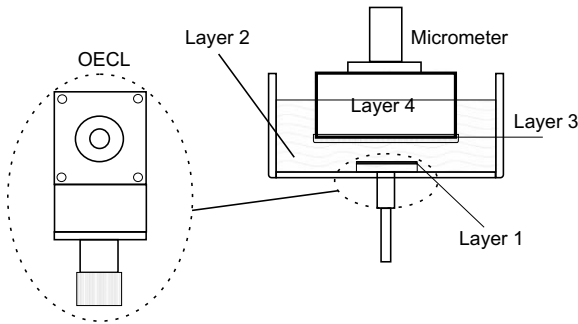


Fig. 6. Non-invasive four layer cell.

In order to obtain C_0 and C_f a calibration of a half-infinite structure was performed first, these data will not be published here.

Identification procedure of a particular four layer calibration structure (nylon film/ water/ nylon film/ 1-butanol with thicknesses $0.01/0.5/0.1/\infty$ mm, respectively) is performed next:

- (1) Estimate the dominant dynamics. Using Eq. (8), $0.03/0.45/0.14$ mm (approximated values of the thicknesses), $\epsilon_1 = \epsilon_2 = 3$ and literature values for water and 1-butanol, the obtained apparent permittivity is

$$\epsilon_{app}^*(s) = \frac{3.4216(s + 3.811 \times 10^{11})(s + 3.45 \times 10^9)}{(s + 8.1 \times 10^{10})(s + 2.894 \times 10^9)}$$

- (2) Find the approximated discrete poles.

$$\zeta_0 = \exp(p_0 T_s) = \exp(-2.894 \times 10^9 s^{-1} 14 \text{ ps}) \approx 0.9621,$$

$$\zeta_1 = \exp(p_1 T_s) = \exp(-8.1 \times 10^{10} s^{-1} 14 \text{ p}) \approx 0.3396.$$

- (3) Generate the bases with Eq. (13): $\mathcal{B}_0(q)$ and $\mathcal{B}_1(q)$.
- (4) Obtain a least square estimate and check the time and frequency Eq. (15) validation parameters. In this example:

$$y_k = \sum_{i=0}^1 \hat{\mathbf{b}}_i \mathcal{B}_i(q) u_k + v_k$$

which can be re-arranged as

$$y_k = \varphi_k^T \hat{\mathbf{b}} = [\mathcal{B}_0(q) u_k, \mathcal{B}_1(q) u_k] \cdot \begin{bmatrix} \hat{\mathbf{b}}_0 \\ \hat{\mathbf{b}}_1 \end{bmatrix},$$

where $\hat{\bullet}$ means “estimate” and $\hat{\mathbf{b}}$ can be analytically solved (see details in [24]).

Repeat the previous steps modifying the parameters in step 1. Results of the whole procedure are shown in Fig. 7. Frequency validation data (see Fig. 7c) show a FIT_f parameter of 86%. Comparison were also performed with theoretical and empirical simulations (Fig. 7d). Good agreement is observed. It should be remarked that

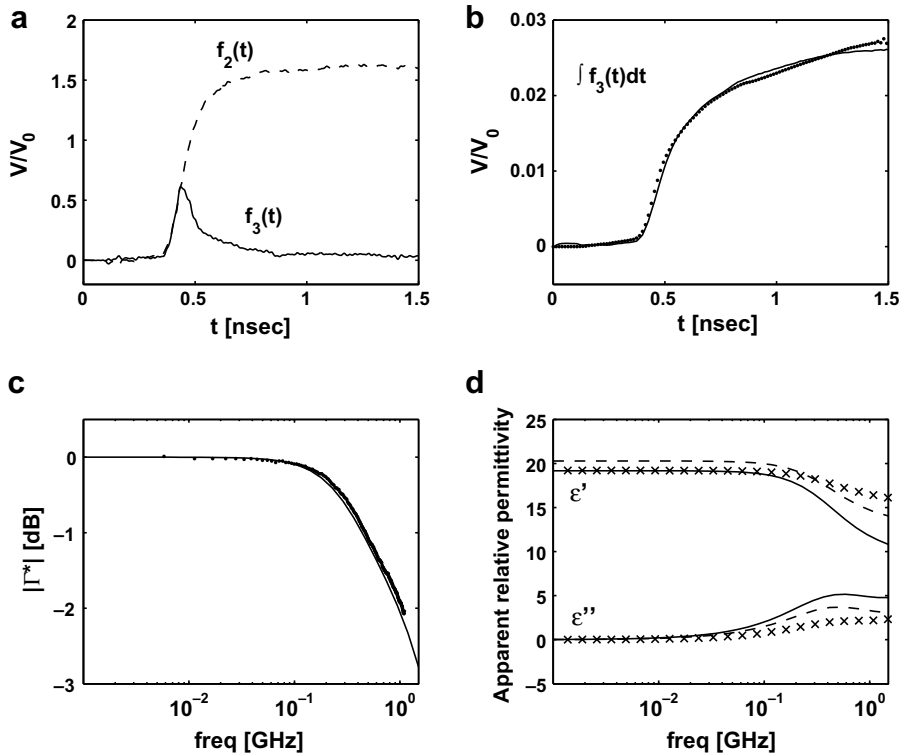


Fig. 7. Calibration procedure in a four layer geometry using a 16 mm probe: nylon film ($d_1 = 0.01$ mm)/water ($d_2 = 0.5$ mm)/nylon film ($d_3 = 0.1$ mm)/ 1-butanol. (a) Filtered time domain measurements. (b) Time domain validation data. Estimated model (full curve) and measured (dotted curve). (c) Frequency domain validation data. Estimated model (full curve) and measured (dotted curve). (d) Complex apparent relative permittivity estimated (full curve), empirical (x curve) and theoretical (dashed curve).

although the frequency relaxation of 1-butanol is 314 MHz (fourth layer), the transfer function has a pole in 460 MHz. Therefore the model and the experiment demonstrate that the whole dynamic of the system does not coincide with the dynamic of a particular layer.

A two layer calibration geometry was also tested, with a thin layer ($d_1 = 0.5$ mm) of an n -alcohol and a second teflon layer (see Table 1).

Fig. 8 shows a comparison between the theoretical, empirical and measured three layered models. Note that results are in relative close agreement up to around 700 MHz. For higher frequencies the accuracy is poor. This may be due to the input signal used. To ensure good identification results, the input signal must excite all the dynamic modes of the system in the frequency range of interest. Unfortunately, as the power components of a step signal decrease with frequency, the “persistence of excitation” condition is not fully guaranteed ([22]).

Table 2 shows the frequency FIT_f parameters obtained in three and four layer calibration media, using the 10 mm and 16 mm probe, respectively. In the three layered experiment, the structure 1 was: water/nylon/ 2-propanol. In structure 2 the first layer was changed to a 0.45% saline solution. In the four layer calibration structure the 16 mm probe was covered with a nylon film and the three layered calibration structure already mentioned were measured again. Fig. 9 shows the four layered structure 2 frequency validation data.

Table 1
Two layer calibration structure compared with the empirical approach using a 10 mm probe (using $q = 0.85$ as empirical parameter)

	Identified			Empirical	
	ϵ_s	ϵ_∞	FIT_f (%)	ϵ_s	ϵ_∞
2-Propanol	11.8	6.2	63	7.9	2.5
1-Butanol	7.5	2.9	68	7.3	2.5
Ethanol	9.8	2.6	63	9.6	3.0

In phantom measurements performed above, time validation FIT_t parameters were always greater than 90%.

4.2. Biological tissue measurement

In addition to the literature application of the multi-layered models [3,4,8,11,12], an illustrative example of a biological measurement is presented next. Measuring in a biological solid inhomogeneous surface (for instance bone surface) has many difficulties. The main problem in solids [28] is the contact between the probe and the material: a small air gap may severely alter the measurement. A solution to this problem may be the application of multi-layer models of OECL, which allow making corrections to experimental data in order to compensate both measurements errors or the effect of layers whose properties are not of interest. Fig. 10a shows a simulation of measuring a solid

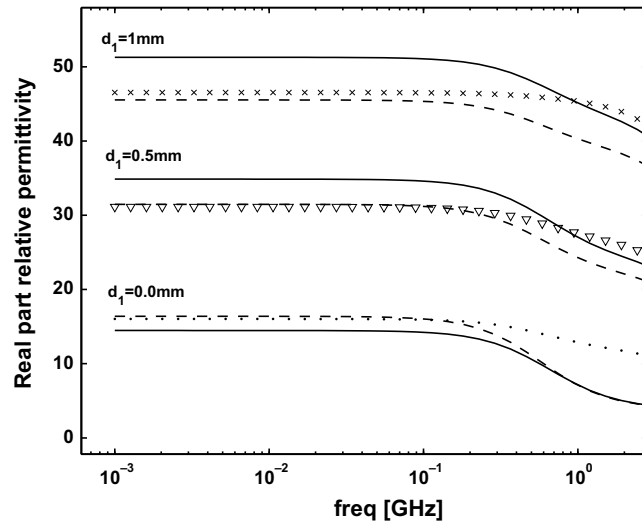


Fig. 8. Comparison between theoretical (full curves), empirical (dashed curves) and measured (\times , ∇ and dotted curves) models. The three layer calibration geometry was: water (with variable thickness)/nylon film ($d_2 = 0.1$ mm)/2-propanol and the 10 mm probe was used.

Table 2
Frequency validation data

d_1 [mm]	3 Layers (10 mm o.d.)			4 Layers (16 mm o.d.)		
	~ 0.0	0.5	1.0	~ 0.0	0.5	1.0
d_2 [mm]	0.1			~ 0.0 0.5 1.0		
Structure 1	75%	74%	84%	81%	82%	78%
Structure 2	50%	55%	62%	51%	72%	61%

FTI_f parameters for the three and four layer calibration media.

with $\epsilon_2 = 15$, in which the air gap is replaced by a thin layer of water ($\epsilon_w = 78$ and $d_1 \simeq 0.5$ mm). It can be seen that the change of $\Delta \epsilon_{app}$ (where $\Delta \epsilon_{app} = \epsilon_{app}(d_1) - \epsilon_{app}(d_1 = 0)$ for air or $\Delta \epsilon_{app} = \epsilon_{app}(d_1) - \epsilon_{app}(d_1 = 0.5)$ for water) is greater in the air case.

Fig. 10b and c show a typical application in cortical bones. Two kind of measurements were compared: invasive (more controlled, see our laboratory previous experiments [2]) and non-invasive. We do not intend to show a biological discussion here, therefore we will briefly describe the sample preparation. For invasive configuration, cortical bovine bones samples were machined into cylinders of 7 mm diameter with a concentric hole of 3 mm diameter. After that, the samples were immersed in bi distilled water and finally thawed just prior to measurements (for details see [2]). For the non-invasive measurements, after carefully removing the periosteum, the tissue was cut into 1 cm cubes. The samples were totally immersed in bidistilled water with a thin water layer ($d_1 \simeq 0.5$ mm) between the 10 mm probe and the sample. The frequency

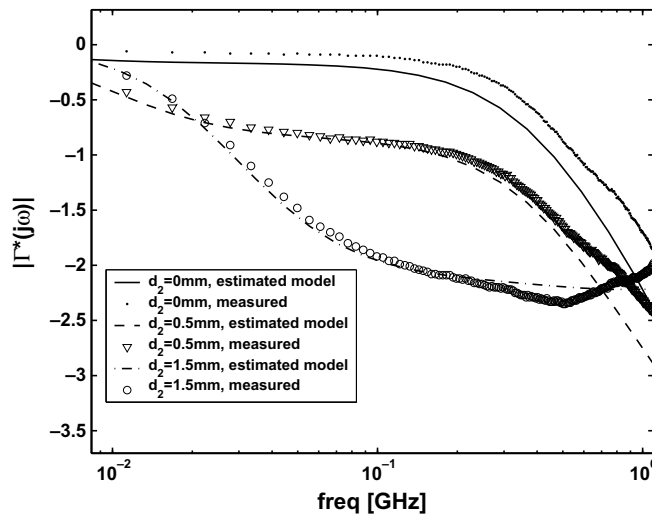


Fig. 9. Frequency validation data for a four layer calibration structure using the 16 mm probe with variable thickness of the second layer: nylon film ($d_1 = 0.01$ mm)/0.45% NaCl solution/nylon film ($d_3 = 0.1$ mm)/ 2-propanol.

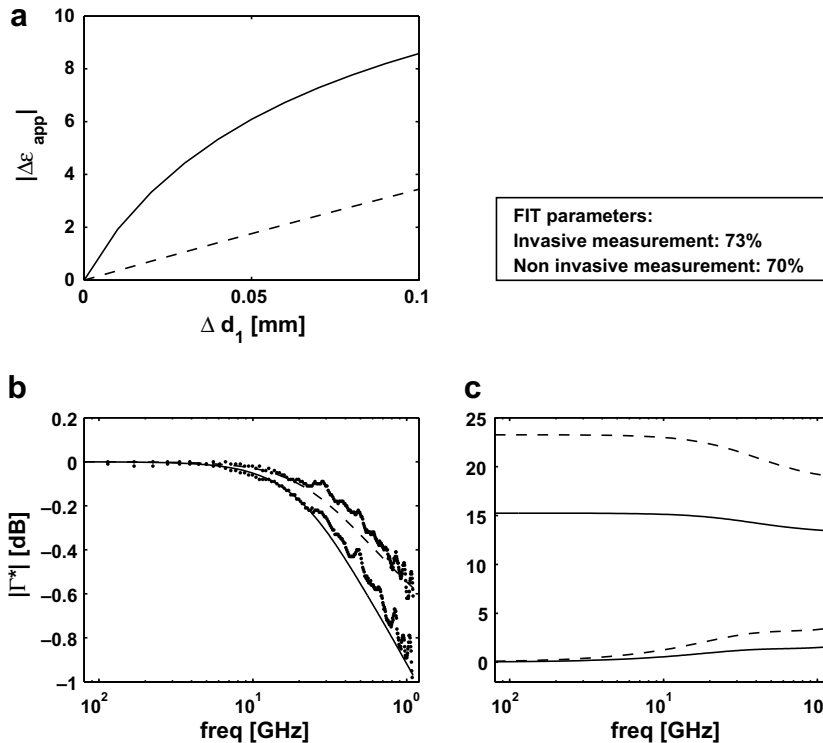


Fig. 10. (a) Simulation of a bi-layered structure: air($\epsilon_1 = 1$)/bone ($\epsilon_2 = 15$) and water ($\epsilon_w = 78$)/bone($\epsilon_2 = 15$), full and dashed curves, respectively. (b) Frequency validation data. (c) Estimated relative permittivity. Invasive (full curves) and non invasive (dashed curves) dielectric measurements in cortical bovine bones.

validation FIT_f parameters are high. Differences in the static value of the permittivity are notorious. It may be due to the high water content of the non-invasive configuration. Relaxation frequencies of both system are in relative good agreement together with their respective $\Delta\epsilon$ parameters.

It should be remarked that the gain of our invasive sensor (a coaxial line filled with the sample as dielectric) is approximately 2.6 times greater than the non-invasive 10 mm probe. Therefore replacing the air by water can be also interpreted as an increment in the gain sensor.

5. Conclusions

The variational formulation of an OECL in contact with a layered geometry was experimentally confirmed with calibration measurements of two, three and four layers. Simple empirical approximations were also tested and generalized showing a relative good agreement. We observed that empirical parameters found by numerical fitting with the variational formulation are, in general, well approximated in calibration measurements.

Orthonormal Bases with Fixed Poles were proposed as a System Identification method to process time domain data. This approach results in a fast and robust measurement configuration. A previous knowledge of the kind of tissue and hence, on the expected values their dielectric properties can take are needed. Therefore, this methodology is

suitable to detect deviations from normal conditions. If the MUM is poorly known, other identification methods can also be applied. On the other hand, non-Debye complex permittivity parameterization are also detectable with this technique at the cost of increasing the model order (see Fig. 5). Some limitations in regard to this topic were summarized in Section 3 together with simulation examples.

Validation of the identified systems were performed in frequency domain. High FIT_f parameters were obtained. It independently demonstrates that good model estimates can be achieved by System Identification methods together with TDR.

As it was shown in Fig. 8, persistence of excitation is not guaranteed for frequencies above 700 MHz, which affects our methodology. Nevertheless, recent advances in the development of very fast pulse generators and fast samplers make the TDR approach a very attractive technique for wide-band analysis. Together with the variational model of the OECL and System Identification methods a relative low cost and robust tool to measure dielectric properties of lossy dielectrics can be obtained.

Finally, we also shown a comparison between a typical invasive and non-invasive measurement of cortical bovine bone. Ulterior studies involving this method as starting point could contribute to a more in-depth knowledge of bone dielectric properties for *in vivo* conditions.

Appendix A. Theoretical formulas for a four layer structure

Definitions of theoretical equations for a four layered structure:

$$P_{ij} = \int_0^{\infty} F_i(\lambda) F_j(\lambda) \frac{1 - R_T e^{-2\lambda d_2}}{1 + R_T e^{-2\lambda d_2}} \lambda^2 d\lambda, \quad (\text{A.1})$$

where R_T is defined as follows:

$$R_T = \frac{R_1 - R_{t_2} e^{-2\lambda d_2}}{1 + R_1 R_{t_2} e^{-2\lambda d_2}} \quad (\text{A.2})$$

and

$$R_{t_2} = \frac{R_2 - R_3 e^{-2\lambda d_3}}{1 + R_2 R_3 e^{-2\lambda d_3}}, \quad (\text{A.3})$$

$$R_i = \frac{\varepsilon_i - \varepsilon_{i+1}}{\varepsilon_i + \varepsilon_{i+1}}, \quad (\text{A.4})$$

where d_i and ε_i are the thickness and the relative complex permittivity of layer i . The rest of the definitions are:

$$F_0(\lambda) = \frac{V_0}{\lambda^2 \ln(a/b)} [J_0(b\lambda) - J_0(a\lambda)],$$

$$F_i(\lambda) = \frac{V_0 p_i^2}{p_i^2 - \lambda^2} \{ b J_0(b\lambda) [\alpha_i J_1(p_i b) + \beta_i Y_1(p_i b)] - a J_0(a\lambda) [\alpha_i J_1(p_i a) + \beta_i Y_1(p_i a)] \}.$$

References

- [1] J. Sierpowska, M.J. Lammi, M.A. Hakulinen, J.S. Jurvelin, R. Lappalainen, J. Toyras, Effect of human trabecular bone composition on its electrical properties, *Med. Eng. Phys.* 29 (2007) 845–852.
- [2] A. Ivancich, J.R. Grigera, C. Muravchik, Electric behaviour of natural and demineralized bones. Dielectric properties up to 1 GHz, *J. Biol. Phys.* 18 (1992) 281–295.
- [3] E. Alanen, T. Lahtinen, J. Nuutinen, Variational formulation of open-ended coaxial line in contact with Layered biological medium, *IEEE Trans. Biomed. Eng.* 45 (1998) 1241–1248.
- [4] E. Alanen, T. Lahtinen, J. Nuutinen, Measurement of dielectric properties of subcutaneous fat with open-ended coaxial sensors, *Phys. Med. Biol.* 43 (1998) 475–485.
- [5] V. Raicu, N. Kitagawa, A. Irimajiri, A quantitative approach to the dielectric properties of the skin, *Phys. Med. Biol.* 45 (2000) L1–L4.
- [6] A. Aimoto, T. Matsumoto, Noninvasive method for measuring the electrical properties of deep tissues using an open-ended coaxial probe, *Med. Eng. Phys.* 18 (8) (1996) 641–646.
- [7] S. Naito, M. Hoshi, S. Yagihara, Microwave dielectric analysis of human stratum corneum in vivo, *Biochim. Biophys. Acta* 1381 (1998) 293–394.
- [8] J. Nuutinen, R. Ikäheimo, T. Lahtinen, Validation of a new dielectric device to assess changes of tissue water in skin and subcutaneous fat, *Physiol. Meas.* 25 (2004) 447–454.
- [9] A. Ivancich, J.R. Grigera, Electric behaviour of natural and demineralized bones, *Stud. Biophys.* 135 (1990) 201–207.
- [10] K. Folger, T. Tjomsland, Permittivity measurement of thin liquid layers using open-ended coaxial probes, *Meas. Sci. Technol.* 7 (1996) 1164–1173.
- [11] S. Bakhtiari, S.I. Ganchev, R. Zoughi, Analysis of radiation from an open-ended coaxial line into stratified dielectrics, *IEEE Trans. Microw. Theory Technol.* 42 (1994) 1261–1267.
- [12] J. Baker-Jarvis, M.D. Janezic, P.D. Domich, G. Geyer, Analysis of an open-ended coaxial probe with lift-off for nondestructive testing, *IEEE Trans. Instrum. Meas.* 43 (1994) 711–718.
- [13] B. García-Bañós, J.M. Catalá-Civera, A.J. Canós, F. Peñaranda-Foix, Design rules for the optimization of the sensitivity of the open-ended coaxial microwave sensors for monitoring changes in dielectric materials, *Meas. Sci. Technol.* 16 (2005) 1186–1192.
- [14] J.R. Mosig, J.E. Besson, M. Gex-Fabry, F.E. Gardiol, Reflection of an open-ended coaxial line and application to nondestructive measurement of materials, *IEEE Trans. Instrum. Meas.* 30 (1981) 46–51.
- [15] L.L. Li, N.H. Ismail, L.S. Taylor, C.C. Davis, Flanged coaxial microwave probes for measuring thin moisture layers, *IEEE Trans. Biomed. Eng.* 39 (1992) 49–57.
- [16] D.K. Misra, M. Chhabra, B.R. Epstein, M. Mirotznik, K.R. Foster, Noninvasive electrical characterization of materials at microwave frequencies using an open-ended coaxial line: test of an improved calibration technique, *IEEE Trans. Microw. Theory Technol.* 38 (1990) 8–14.
- [17] T.W. Athey, M.A. Stuchly, S.S. Stuchly, Measurement of radio frequency permittivity of biological tissues with an open-ended coaxial line: Part I, *IEEE Trans. Microw. Theory Technol.* MTT-30 (1982) 82–86.
- [18] D. Popovic, L. McCartney, C. Beasley, M. Lazebnik, M. Okoniewski, S.C. Hagness, J.H. Booske, Precision open-ended coaxial probes for in vivo and ex vivo dielectric spectroscopy of biological tissues at microwave frequencies, *IEEE Trans. Microw. Theory Technol.* 53 (5) (2005) 1713–1722.
- [19] R.H. Cole, J.G. Berberian, S. Mashimo, G. Chrystoskos, A. Burns, E. Tombari, Time domain reflection methods for dielectric measurements to 10 GHz, *J. Appl. Phys.* 66 (2) (1989) 793–802.
- [20] A. Bennis, N.S. Nahman, Deconvolution of causal pulse and transient data, *IEEE Trans. Instrum. Meas.* 39 (1990) 933–939.
- [21] P. Ferrari, G. Angénioux, Calibration of a time-domain network analyzer: a new approach, *IEEE Trans. Instrum. Meas.* 49 (2000) 178–187.
- [22] L. Ljung, *System Identification: Theory for the User*, second ed., Prentice-Hall, Inc., Englewood, Cliffs, NJ, 1999.
- [23] L. Ljung, *System Identification Toolbox, User's Guide*, ver. 5, The MathWorks, Inc., Natick, MA, 2000.
- [24] J.C. Gómez, Analysis of dynamic system identification using rational orthonormal bases, Ph.D. Thesis, The University of Newcastle, Australia, PS file downloadable from <<http://www.fceia.unr.edu.ar/~jcgomez>>.
- [25] Yu.D. Feldman, Yu.F. Zuev, I.V. Ermolina, V.A. Goncharov, Difference method of analysing dielectric data in the time domain, *Russ. J. Phys. Chem.* 62 (2) (1988) 269–271.
- [26] T. Shinomiya, Dielectric dispersion and intermolecular association for 28 pure liquid alcohols. The position dependence of hydroxyl group in the hydrocarbon chain, *Bull. Chem. Soc. Jpn.* 62 (1989) 908–914.
- [27] R. Hilfer, H-function representations for stretched exponential relaxation and non-Debye susceptibilities in glassy systems, *Phys. Rev. E* 65 (2002) 061510–061511.
- [28] R. Olmi, M. Bini, A. Ignesti, C. Riminesi, Non-destructive permittivity measurement of solid materials, *Meas. Sci. Technol.* 11 (2000) 1623–1629.